

## Research Article

Shwetabh Verma, Juergen Hesser and Samuel Arba-Mosquera\*

# Effect of laser beam truncation (pinhole), (ordered) dithering, and jitter on residual smoothness after poly(methyl methacrylate) ablations, using a close-to-Gaussian beam profile

<https://doi.org/10.1515/aot-2021-0040>

Received August 18, 2021; accepted September 24, 2021;  
published online October 15, 2021

**Abstract:** Smoother surfaces after laser vision correction have been widely accepted as a factor for improving visual recovery regardless of the used technique (PRK, LASIK, or even SMILE). We tested the impact of laser beam truncation, dithering (expressing a continuous profile on a basis of lower resolution causing pixels to round up/down the number of pulses to be placed), and jitter (a controlled random noise (up to  $\pm 20 \mu\text{m}$  in either direction) added to the theoretical scanner positions) on residual smoothness after Poly(methyl methacrylate) (PMMA) ablations, using a close-to-Gaussian beam profile. A modified SCHWIND AMARIS system has been used providing a beam profile with the following characteristics: close-to-Gaussian beam profile with full width at half maximum (FWHM) of  $540 \mu\text{m}$ , 1050 Hz. Laser parameters have been optimized following *Invest. Ophthalmol. Vis. Sci.*, vol. 58, no. 4, pp. 2021–2037, 2017, the pulse energy has been optimized following *Biomed. Opt. Express* vol. 4, pp. 1422–1433, 2013. For the PMMA ablations, two configurations (with a 0.7 mm pinhole and 0.75 mJ and without pinhole and 0.9 mJ (for fluences of  $329 \text{ mJ}/\text{cm}^2$  and  $317 \text{ mJ}/\text{cm}^2$  and corneal

spot volumes of 174 and 188 pl)) were considered, along with two types of lattices (with and without ordered dithering to select the optimum pulse positions), and two types of spot placement (with and without jitter). Real ablations on PMMA (ranging from  $-12\text{D}$  to  $+6\text{D}$  with and without astigmatism of up to 3D) completed the study setup. The effect of the  $2 \times 2 \times 2$  different configurations was analyzed based on the roughness in ablation estimated from the root mean square error in ablation. Truncation of the beam is negatively associated to a higher level of residual roughness; ordered dithering to select the optimum pulse positions is positively associated to a lower level of residual roughness; jitter is negatively associated to a higher level of residual roughness. The effect of dithering was the largest, followed by truncation, and jitter had the lowest impact on results. So that: Dithering approaches help to further minimize residual roughness after ablation; minimum (or no) truncation of the beam is essential to minimize residual roughness after ablation; and jitter shall be avoided to minimize residual roughness after ablation. The proposed model can be used for optimization of laser systems used for ablation processes at relatively low cost and would directly improve the quality of results. Minimum (or no) truncation of the beam is essential to minimize residual roughness after ablation. Ordered dithering without jitter helps to further minimize residual roughness after ablation. Other more complex dithering approaches may further contribute to minimize residual roughness after ablation.

**Keywords:** ablation roughness; dithering; Gaussian order; jitter; spot overlap; truncation radius.

A preliminary version of this work has been presented during ARVO 2019 Annual Meeting on May 2nd 2019 in Vancouver.

\*Corresponding author: Samuel Arba Mosquera, Research and Development, SCHWIND eye-tech-solutions, Mainparkstrasse 6-10, D-63801, Kleinostheim, Germany, Phone: +49 6027 508 274, E-mail: samuel.arba.mosquera@eye-tech.net. <https://orcid.org/0000-0002-3152-0557>

Shwetabh Verma, Research and Development, SCHWIND eye-tech-solutions, Kleinostheim, Germany

Juergen Hesser, Experimental Radiation Oncology, University Medical Center Mannheim, Heidelberg University, Heidelberg, Germany; Interdisciplinary Center for Scientific Computing (IWR), Heidelberg University, Heidelberg, Germany; and Central Institute for Computer Engineering (ZITI), Heidelberg University, Heidelberg, Germany

## 1 Introduction

Lasers with small laser spots and high repetition rates are now widely used to manipulate the shape of the cornea to correct refractive errors. Achieving accurate clinical outcomes and reducing the likelihood of a retreatment procedure are major goals of refractive surgery. Despite a

myriad of technological advances in this field, laser corneal refractive surgery still presents some challenges in achieving higher ablation smoothness and minimizing the applied energy on the cornea. The temporal and spatial distribution of the laser spots (scan sequence) has shown to affect the surface quality and maximum ablation depth of the ablation profile. Smoothness of ablation may also vary with different excimer lasers systems [1]. In a study, ablations were performed on Poly(methyl methacrylate) (PMMA) plates, with four different excimer lasers: VISX-Star, Coherent Schwind Keratom I/II, Chiron Technolas Keracor 117C (Plano Scan), and the Nidek EC-5000, to determine and compare the homogeneity and smoothness of the surface. It was concluded that the laser with Scanning spot technology produced smooth ablations even up to  $-9.00$  D. Ablation smoothness is also influenced by spot positioning algorithms. Dago et al. performed ablations on PMMA plates using four scanning excimer lasers, two with flying spot technology (Zeiss-Meditec MEL-70, and a Russian-made unit, Microscan) and two Nidek models with scanning slit delivery systems and an expanding iris diaphragm (EC-5000 and EC-5000 CX) [2]. The smoothest surface was obtained in samples produced by Zeiss-Meditec MEL-70 unit ( $\text{RMS} = 112 \pm 23$  nm), followed by the Nidek EC-5000 CX ( $\text{RMS} = 153 \pm 12$  nm), and the Microscan ( $\text{RMS} = 181 \pm 11$  nm). It was concluded that scanning excimer lasers based on flying spot technology created smoother ablations on PMMA plates compared to the older Nidek EC-5000 unit.

It has been theoretically shown that corneal laser surgery could benefit from smaller spot sizes and higher repetition rates [3, 4]. Furthermore, higher refractive settings correlate with decreasing surface smoothness. These results have been reproduced in PMMA by O'Donnell et al. [5], showing an increase of 25 nm roughness per micron of ablation in PMMA.

Figure 1 shows an oversimplified sketch of how roughness is induced during the pulse-by-pulse ablation process.

An analytical model was proposed to optimize the ablation efficiency based on different metrics of ablation derived from the modification in the Beer–Lambert's law [6] followed by a theoretical framework for determining the optimum laser beam characteristics for achieving smoother ablations in laser vision correction [7]. Extending this model, the main purpose of this paper is to provide empirical results of the impact of laser beam characteristics like truncation radius, lattice arrangement, and jitter on ablation smoothness measured as residual roughness in PMMA plates after being ablated with an excimer laser system.

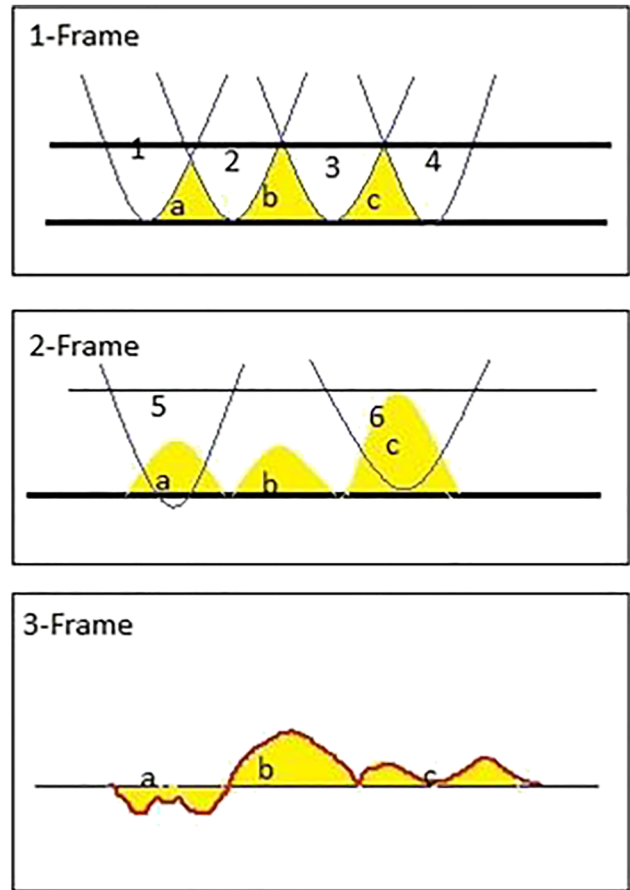


**Figure 1:** Schematic representation of how the roughness is induced during the pulse-by-pulse ablation process – exaggerated scale.

## 2 Methods

A modified SCHWIND AMARIS system has been used providing a beam profile with the following characteristics: full width at half maximum (FWHM) of  $540 \mu\text{m}$ , super-Gaussian order ( $N$ ) of 1.27, and repetition rate of 1050 Hz. The laser parameters and the pulse energy have been optimized following previous works [6, 7]. For PMMA ablations, two configurations (with a  $0.7$  mm pinhole and  $0.75$  mJ and without pinhole and  $0.9$  mJ (for fluences of  $329$  mJ/cm<sup>2</sup> and  $317$  mJ/cm<sup>2</sup> and corneal spot volumes of 174 and 188 pl)) were considered, along with two types of lattices (with and without ordered dithering to select the optimum pulse positions), and two types of spot placement (with and without jitter).

### 2.1 Truncation (pinhole)

Roughness in ablation was measured with (standard setting) versus without truncation ( $0.7$  mm diameter, corresponding to 76% transmission, and 27% cut-off at the flanks).

The effect of Pinhole on radiant exposure, estimated ablation depth on the cornea and PMMA is displayed in Figure 2.

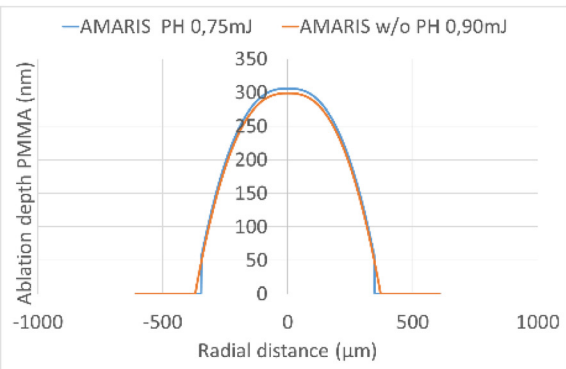
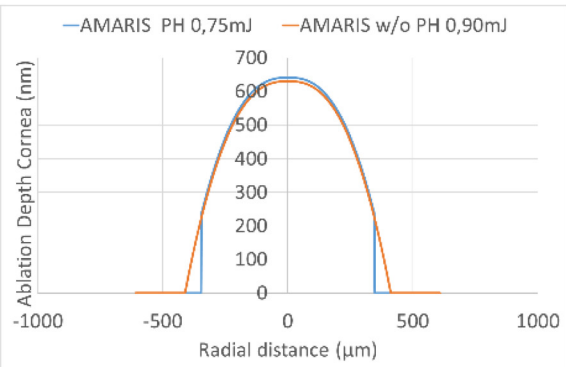
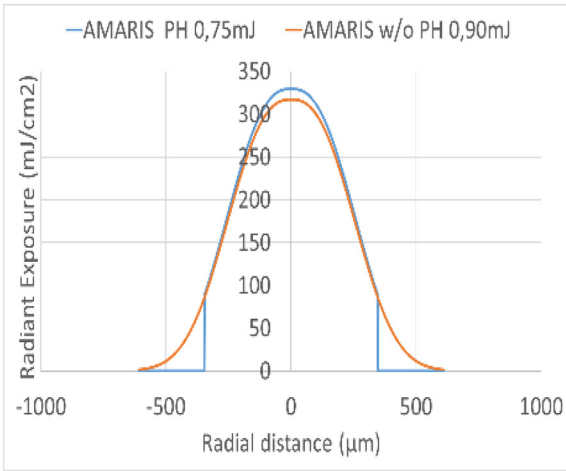
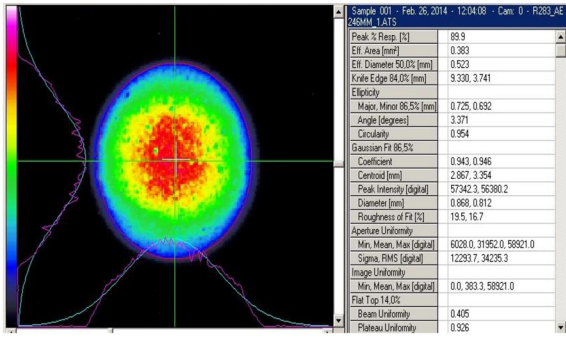


**Figure 2:** Top: Measured beam profile of the used laser system in the presence of a 0.7 mm pinhole. Bottom: Simulated theoretical effect of pinhole truncating the 0.82 mm beam to a 0.7 mm spot. Essentially the pinhole cuts-off the flanks of the spot, reducing the

## 2.2 Ordered dithering lattice geometry

Ordered dithering is an image dithering algorithm. It is commonly used to display a continuous image on a display of smaller color depth. The algorithm reduces the number of colors (without applying pseudo-gray, or bit-stealing [8]) by applying a threshold map  $M$  to the pixels displayed, causing some pixels to change color, depending on the distance of the original color from the available color entries in the reduced palette. This threshold map (for sides with length as power of two) is also known as an index matrix or Bayer matrix [9].

Arbitrary size threshold maps can be devised with a simple rule: First fill each slot with successive integers. Then reorder them such that the average distances between two successive numbers in the map is as large as possible, ensuring that the table “wraps” around at edges.

The algorithm renders the image normally, but for each pixel, it adds a value from the threshold map, causing the pixel’s value to be quantized one step higher if it exceeds the threshold. For example, in monochrome rendering, if the value of the pixel is less than the number in the corresponding cell of the matrix, plot that pixel black, otherwise, plot it white.

The size of the map selected should be equal to or larger than the ratio of source colors to target colors. For example, when quantizing a 24 bpp image to 15 bpp (256 colors per channel to 32 colors per channel), the smallest map one would choose would be  $4 \times 2$ , for the ratio of 8 (256:32). This allows expressing each distinct tone of the input with different dithering patterns.

Bayer has shown that for matrices of orders which are powers of two there is an optimal pattern of dispersed dots which results in the pattern noise being as high-frequency as possible.

The idea behind it is simple: given two available values  $a$  and  $b$ , let’s say black and white, the value  $x$  between  $a$  and  $b$ —that should be grayish—is simulated by mixing pixels of colors  $a$  and  $b$ . To apply some ordered dithering on an image, we apply the same logic but in 2D by using a Bayer matrix. By turning the pixel on in a very specified order, the matrix creates the perception of continuous variation of color. In these matrices, consecutive threshold values are located far apart spatially, which gives the perception of a progressive variation.

This concept can be easily adapted to the discretization of an ablation volume into an integer collection of pulses per position. The task is now to express a continuous profile on basis smaller resolution. The algorithm causes some pixels to round up the number of pulses to be placed, and some others to round down. The size of the map selected should be equal to or larger than the ratio of the size of the ablation profile to the size of the spot (building block).

## 2.3 Jitter

In optics, the term jitter is used to refer to the oscillatory motion of the image with respect to the detector, which blurs the image. In our case, it is a controlled random noise (up to  $\pm 20 \mu\text{m}$  in either direction) added to the theoretical scanner positions. This may help avoiding/breaking patterned effects in the overlapped spots. As expressed in the history of PRK [10]:

total energy of the pulse at the expense of inducing high frequency signals. The peak radiant exposure (related to the pulse energy) of the beam without pinhole has been slightly reduced to keep a good comparison in the per pulse ablation volume on corneal tissue and PMMA.

The researchers began working in a trailer at Luisiana State University that was next to a trash compactor, which inadvertently led to a discovery. The researchers found that when the trash compactor was operating, it shook the trailer, which made the laser wobble instead of shooting straight down into the patient’s eye. McDonald said that when the trailer was not vibrating, the treatments were not as smooth and the results not as good. This led to a smoothing of the procedure so the ridges the laser produced were eliminated.

Real ablations on PMMA (ranging from -12D to +6D with and without astigmatism of up to 3D) completed the study setup. The various test conditions are presented in Table 1. For each test condition, a total of 12 ablations were performed on PMMA, and the average

**Table 1:** Summary of the various test settings. Here for Pinhole, ‘Y’ represents truncation of the laser beam using a pinhole (0.7 mm diameter) and ‘N’ represents no truncation (and for Energy, ‘Y’ represents 0.75 mJ and ‘N’ represents 0.9 mJ); for Dithering, ‘Y’ represents use of lattice with ordered dithering to select the optimum pulse positions and ‘N’ represents lattice without ordered dithering; for Jitter, ‘Y’ represents a controlled random noise (up to ±20 µm in either direction) added to the theoretical scanner positions while ‘N’ represents no random noise.

Test number	Pinhole (Energy)	Dithering	Jitter
1	Y	N	N
2	Y	N	Y
3	Y	Y	Y
4	Y	Y	N
5	N	Y	N
6	N	Y	Y
7	N	N	Y
8	N	N	N

efficiency (Achieved ablation/Expected ablation as described in previous works [11]) and induced ablation roughness were considered as the primary outcomes.

To determine the individual measurements, a laser scanning deflectometer (SCHWIND PMMA Profilometer, SCHWIND eye-tech-solutions GmbH) was used [12].

The mean ablation performance is a relative measure of the ablation performance that is nondimensional. Second-order (low-order) Zernike coefficients and fourth-order Zernike coefficients were used, creating a value similar to a Seidel refraction. The mean ablation performance was defined as the mean value, and the ablation variability was defined as the standard deviation (SD) of the 12 individual measurements for each test condition. The mean performance is related to the slope of a linear fit achieved versus attempted correction power.

The roughness induced by the ablation was estimated from the root mean square (RMS) error in ablation. This method is essentially the same used in previous works [3], the roughness (RMS of ablation irregularities) was calculated from the derived ablation profiles by applying a fourth-order Zernike fit to subtract the underlying shape of the ablation profile. The residual fluctuations were statistically analyzed within the treatment zone to derive the ablation roughness. Figure 3 depicts the determination of roughness for 2 cases of same dioptric power but different induced ablation roughness.

The effect of the 2 × 2 × 2 different configurations (two states of Pinhole, two sates of lattice order dithering, and two states of jitter spot placement) was analyzed based on the roughness in ablation estimated from the root mean square error in ablation.

An empirical comparison model was set for evaluating the roughness induced by the ablation process, following the methodology as:

- (1) Set high and low fluence parameters to the same energy (0.75 mJ) at the working plane (single fluence)
- (2) Perform a fluence test and a PMMA test (Test 1: pinhole, w/o dithering, w/o jitter)
- (3) Enable jitter = 20 µm

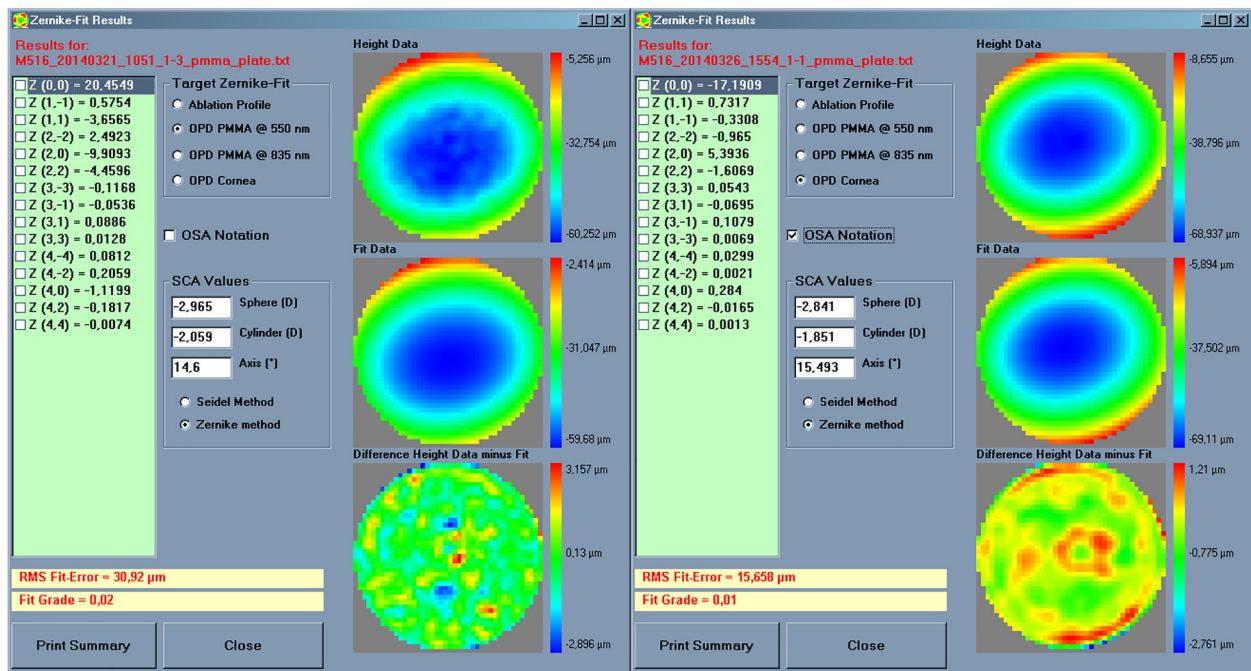


**Figure 3:** Example of roughness of a PMMA test performed with two different configurations, leading to different levels of roughness.

- (4) Perform a fluence test and a PMMA test (Test 2: pinhole, w/o dithering, jitter)
- (5) Enable dithering
- (6) Perform a fluence test and a PMMA test (Test 3: pinhole, dithering, jitter)
- (7) Disable jitter
- (8) Perform a fluence and a PMMA test (Test 4: pinhole, dithering, w/o jitter)
- (9) Remove the pinhole
- (10) Set high and low fluence parameters to the same energy (0.9 mJ) at the working plane (single fluence)
- (11) Perform a fluence and a PMMA test (Test 5: w/o pinhole, dithering, w/o jitter)
- (12) Enable jitter = 20  $\mu\text{m}$
- (13) Perform a fluence and a PMMA test (Test 6: w/o pinhole, dithering, jitter)
- (14) Disable dithering
- (15) Perform a fluence and a PMMA test (Test 7: w/o pinhole, w/o dithering, jitter)
- (16) Disable jitter
- (17) Perform a fluence and a PMMA test (Test 8: w/o pinhole, w/o dithering, w/o jitter)
- (18) Reset system to standard AMARIS
  - This corresponds to a nonsequential settings procedure to avoid/reduce model bias; time drifts, hysteresis effects.

## 2.4 PMMA tests

Eight PMMA Tests have been performed (each consisting of 12 ablations ranging from  $-12\text{D}$  to  $+6\text{D}$ ) and analyzed from a single AMARIS system. These conformed a  $2 \times 2 \times 2$  matrix comparing with versus without pinhole, dithering, and jitter. Mean performance values with standard deviations [11, 12], and roughness [3, 7] have been evaluated. To increase robustness  $8 \times 8$  analyses, four vs. four cumulative analyses, as well as pairwise analyses have been included.

## 3 Results

In general, truncation of the beam is negatively associated to a higher level of residual roughness; ordered dithering to select the optimum pulse positions is positively associated to a lower level of residual roughness; jitter is negatively associated to a higher level of residual roughness. The effect of dithering was the largest, followed by truncation, and jitter had the lowest impact on results. So that: dithering approaches help to further minimize residual roughness after ablation; minimum (or no) truncation of the beam is essential to minimize residual roughness after ablation; and jitter shall be avoided to minimize residual roughness after ablation.

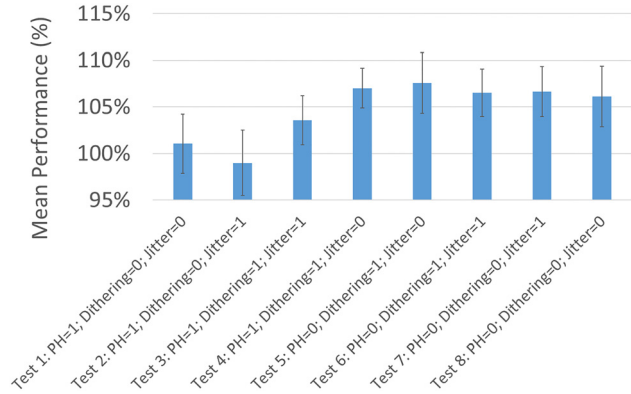


**Figure 4:** Mean performance measured for each test condition, ranging from 99 to 108%.

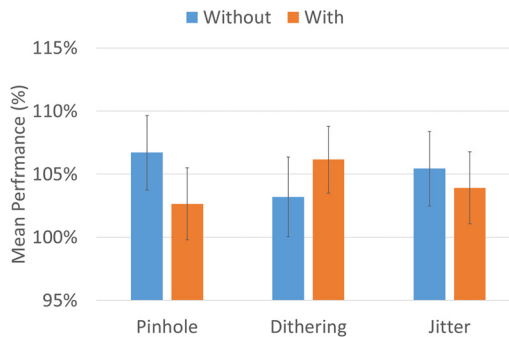


**Figure 5:** Four vs. four cumulated comparison of the effects of pinhole, dithering, and jitter on mean ablation performance on PMMA. The absence of pinhole enhanced performance by +4% ( $p < 0.005$ ); the use of ordered dithering enhanced performance by +3% ( $p < 0.01$ ); and the absence of jitter enhanced performance by +1% ( $p < 0.05$ ).

### 3.1 Mean performance

Performance for all eight test settings is displayed in Figure 4, whereas cumulative effect of pinhole, dithering, and jitter is displayed in Figure 5. The absence of pinhole enhanced performance by +4% ( $p < 0.005$ ); the use of ordered dithering enhanced performance by +3% ( $p < 0.01$ ); and the absence of jitter enhanced performance by +1% ( $p < 0.05$ ).

### 3.2 Roughness

Roughness for all eight test settings is displayed in Figure 6, whereas cumulative effect of pinhole, dithering,

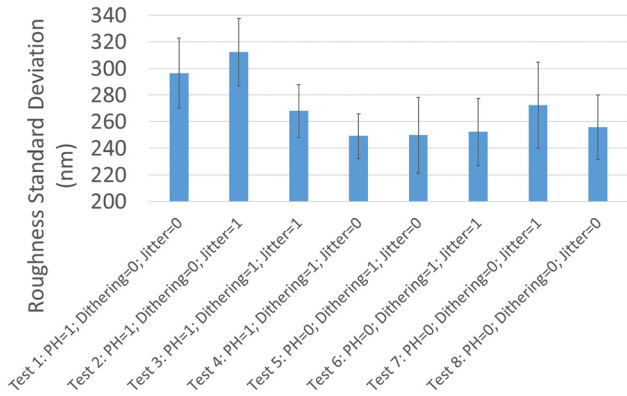


**Figure 6:** Residual roughness measured for each test condition, ranging from 160 to 427 nm.

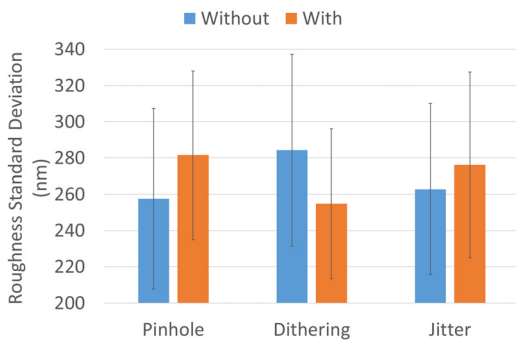


**Figure 7:** Four vs. four cumulated comparison of the effects of pinhole, dithering, and jitter on residual roughness on PMMA. The absence of pinhole reduced roughness by  $-8\%$  ( $p < 0.00,005$ ); the use of ordered dithering reduced roughness by  $-11\%$  ( $p < 0.00,001$ ); and the absence of jitter reduced roughness by  $-4\%$  ( $p < 0.0005$ ).

and jitter is displayed in Figure 7. The absence of pinhole reduced roughness by  $-8\%$  ( $p < 0.00,005$ ); the use of ordered dithering reduced roughness by  $-11\%$  ( $p < 0.00,001$ ); and the absence of jitter reduced roughness by  $-4\%$  ( $p < 0.0005$ ).

### 3.3 Roughness versus ablation depth

The relationship roughness (in the form of sum of the squared residuals) versus maximum ablation depth is displayed in Figure 8 for pinhole, dithering, and jitter. It followed a power function, with an exponent  $\sim 1.4-1.5$  with maximum ablation depth providing reasonable  $R^2 > 0.8$ . The best fit lines confirm that the absence of pinhole, the use of ordered dithering, and the absence of jitter all reduced roughness.

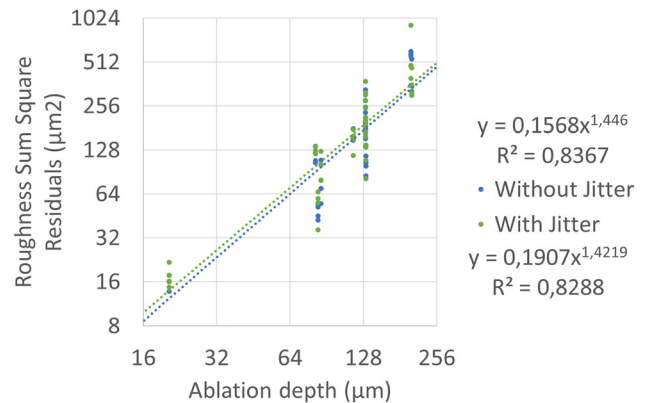
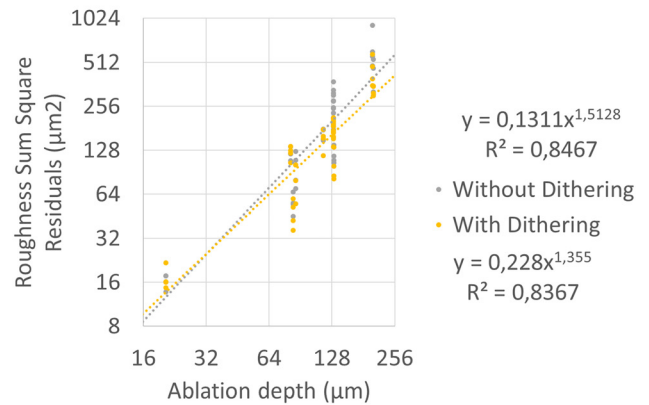
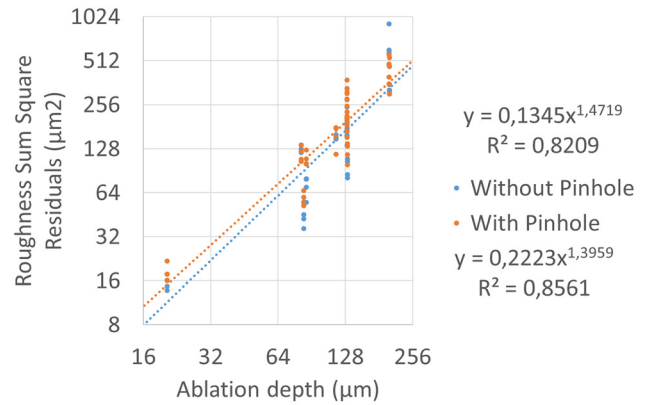


**Figure 8:** Roughness (expressed as the sum of squared residuals) versus maximum ablation depth in a four vs. four cumulated comparison of the effects of pinhole (top), dithering (centre), and jitter (bottom). It follows a power function, with an exponent  $\sim 1.4-1.5$  with maximum ablation depth providing reasonable  $R^2 > 0.8$ . The best fit lines confirm that the absence of pinhole, the use of ordered dithering, and the absence of jitter all reduced roughness.

### 3.4 Pairwise comparisons

Pairwise comparisons are shown in Table 2. The pairwise comparisons confirm that for all but one case the absence

**Table 2:** Pairwise comparisons: the absence of pinhole, the use of ordered dithering, and the absence of jitter all reduced roughness.

Pairwise	Test	RMS ± SD (nm)	Counterpart Test	RMS ± SD (nm)	Comparison (bold Statistically significant)
Pinhole	Test 1: PH = 1; Dithering = 0; Jitter = 0	297 ± 26	Test 8: PH = 0; Dithering = 0; Jitter = 0	256 ± 24	<b>No PH better</b>
	Test 2: PH = 1; Dithering = 0; Jitter = 1	312 ± 25	Test 7: PH = 0; Dithering = 0; Jitter = 1	272 ± 32	<b>No PH better</b>
	Test 3: PH = 1; Dithering = 1; Jitter = 1	268 ± 20	Test 6: PH = 0; Dithering = 1; Jitter = 1	252 ± 25	No PH better
	Test 4: PH = 1; Dithering = 1; Jitter = 0	249 ± 17	Test 5: PH = 0; Dithering = 1; Jitter = 0	250 ± 28	PH better
Dithering	Test 3: PH = 1; Dithering = 1; Jitter = 1	268 ± 20	Test 2: PH = 1; Dithering = 0; Jitter = 1	312 ± 25	<b>Dithering better</b>
	Test 4: PH = 1; Dithering = 1; Jitter = 0	249 ± 17	Test 1: PH = 1; Dithering = 0; Jitter = 0	297 ± 26	<b>Dithering better</b>
	Test 5: PH = 0; Dithering = 1; Jitter = 0	250 ± 28	Test 8: PH = 0; Dithering = 0; Jitter = 0	256 ± 24	Dithering better
	Test 6: PH = 0; Dithering = 1; Jitter = 1	252 ± 25	Test 7: PH = 0; Dithering = 0; Jitter = 1	272 ± 32	<b>Dithering better</b>
Jitter	Test 2: PH = 1; Dithering = 0; Jitter = 1	312 ± 25	Test 1: PH = 1; Dithering = 0; Jitter = 0	297 ± 26	<b>No jitter better</b>
	Test 3: PH = 1; Dithering = 1; Jitter = 1	268 ± 20	Test 4: PH = 1; Dithering = 1; Jitter = 0	249 ± 17	<b>No jitter better</b>
	Test 6: PH = 0; Dithering = 1; Jitter = 1	252 ± 25	Test 5: PH = 0; Dithering = 1; Jitter = 0	250 ± 28	No jitter better
	Test 7: PH = 0; Dithering = 0; Jitter = 1	272 ± 32	Test 8: PH = 0; Dithering = 0; Jitter = 0	256 ± 24	<b>No jitter better</b>

of pinhole, the use of ordered dithering, and the absence of jitter all reduced roughness.

### 3.5 Best-worst comparisons

The rank of residual roughness is shown in Table 3. The worst condition (Figure 6) was test setting 2 (with pinhole, without dithering, and with jitter) as exactly predicted by Figures 7 and 8 (and Table 2). Its counterpart, derived as best from Figures 7 and 8 (and Table 2) would be test setting 5 (without pinhole, with dithering, and without jitter), but the actual empirical best condition (Figure 6) was Test setting 4 (with pinhole, with dithering, and without jitter). These three settings are displayed and analyzed in Figure 9. There was no statistically significant difference in roughness between test settings 4 and 5 (empirical best vs. predicted best) (difference in roughness 0.1%;  $p = 0.5$ ). There was a clear statistically significant difference in roughness between test setting 2 and test settings 4 and 5 (worst vs. best) (difference in roughness +24%;  $p < 0.00,001$ ). The same holds for the relationship roughness (in the form of sum of the squared residuals) versus

**Table 3:** Rank for the residual roughness on PMMA.

Rank	Test
1	Test 4: PH = 1; Dithering = 1; Jitter = 0
2	Test 5: PH = 0; Dithering = 1; Jitter = 0
3	Test 6: PH = 0; Dithering = 1; Jitter = 1
4	Test 8: PH = 0; Dithering = 0; Jitter = 0
5	Test 3: PH = 1; Dithering = 1; Jitter = 1
6	Test 7: PH = 0; Dithering = 0; Jitter = 1
7	Test 1: PH = 1; Dithering = 0; Jitter = 0
8	Test 2: PH = 1; Dithering = 0; Jitter = 1

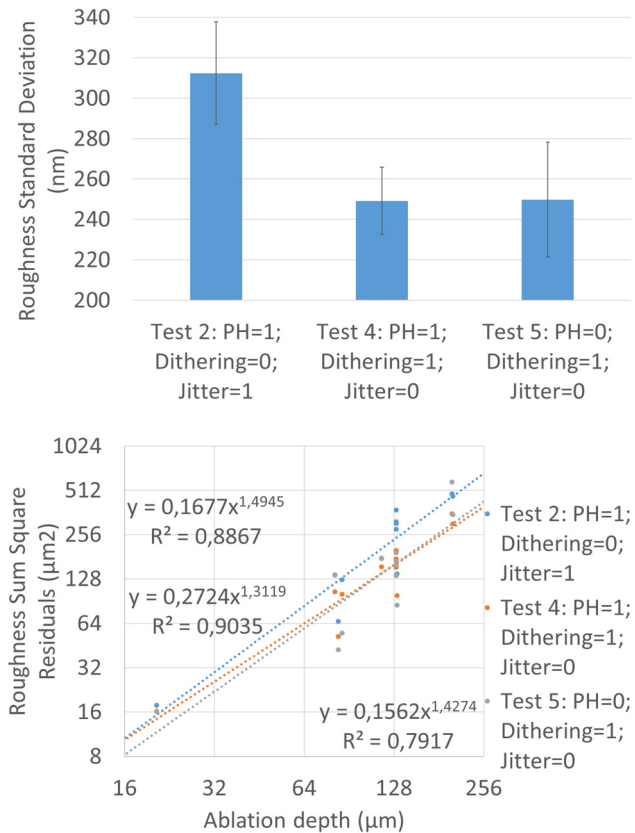


**Figure 9:** Worst-best comparisons: The absence of pinhole, the use of ordered dithering, and the absence of jitter all reduced roughness. There was no statistically significant difference in roughness between test settings 4 and 5 (empirical best vs. predicted best) (difference in roughness 0.1%;  $p = 0.5$ ). There was a clear statistically significant difference in roughness between test setting 2 and test settings 4 and 5 (worst vs. best) (difference in roughness +24%;  $p < 0.00,001$ ). The same holds for the relationship roughness (in the form of sum of the squared residuals) versus maximum ablation depth, which is largely overlapped for test settings 4 and 5 (best), and distinctly higher for test setting 2.

**Table 4:** Consolidated summary.

Conditions without jitter//with jitter = 20 $\mu\text{m}$	0.7 mm pinhole and 0.75 mJ energy	No pinhole and 0.9 mJ energy
Heuristic reticular search	Baseline (100% residual roughness)//+5%	-8%// -4%
Ordered dithering search	-11%// -7%	-18%// -14%

maximum ablation depth, which is largely overlapped for test settings 4 and 5 (best), and distinctly higher for test setting 2.

### 3.6 Summary

For the input parameters presented in Table 1, a proper optimum configuration for minimizing the roughness is summarized in Table 4.

## 4 Discussion

The obtained results are not surprising and confirm the theoretical and simulated predictions [7]. Beyond the confirmation, this work provides a quantification of the effects (for the described settings).

Cutting off the intensity (truncation through e.g., a pinhole) introduces a sharp edge that cannot be compensated otherwise and hence roughness is increased. It could be expected that gradual intensity absorption to achieve a smooth laser spot profile would overcome this problem. The pinhole in the AMARIS system lies in a meta-focus, in a position/plane conjugated to the ablation plane, but the pinhole is not the focus. So that the Gaussian focusing optics may actually create a flank (instead of a sharp-edge) out of the pinhole (Figure 2 Top).

Jitter adds random noise while partially reducing the residual. This is equivalent to increase the variance and hence increases roughness. This may not be the theoretical case for jitter applied to pinhole/truncated beams (as the history shows) [10]. Jitter would then smoothen the sharp truncation into a (Gaussian) progressive flank (in the limiting case as the convolution of the single spot shape with the jitter random function).

Dithering is constructed in such a way that there may be a (very) high frequency contribution to roughness (with the reciprocal of the minimum interspot distance as frequency) but a near optimal compromise to achieve the desired ablation profile (small amplitude of the roughness “signal”). The latter is responsible for minimizing the variance. In a sense, it could be argued that the roughness

is not reduced, but rather sent to frequencies out of the measurement relevant spectrum.

The roughness in ablation after refractive surgery is related to the transmission of light in the cornea [13]. Perez–Merino et al. [14] analyzed the relationship among transmittance, scattering and epithelial surface properties during wound healing after refractive surgery in hens operated using different refractive surgery techniques (Lasik, Lasek, PRK). Their results suggested that higher roughness in the epithelium-stroma interface causes a decrease of transmittance and an increase of scattering. Larger differences between internal and external roughness of epithelium contributes to produce a decrease of transmittance and an increase of scattered light.

Various measurement techniques have been developed for the measurements of surface roughness [15]. To test the effect of radiant exposure on surface smoothness, Fantes et al. [16] ablated rabbit corneas with the 193 nm argon fluoride excimer laser at nine radiant exposures from 50 to 850 mJ/cm<sup>2</sup>. They showed that the uniformity of the surface following laser ablation may play an important role in the rate of epithelial healing and amount and type of stromal scarring. It has been experimentally shown that high levels of surface roughness produced by some laser systems may be sufficient to degrade visual performance under some circumstances [17]. O’Donnell et al. [5] showed that surface irregularities in PMMA increase with ablation depth and proposed a unit of measure of roughness expressed as the peak-to-valley distance in ablation. The excimer laser interacts with the non-ablated residual stromal surface in a characteristic fashion not seen with isotropic, inorganic material. McCafferty et al. [18] postulated that the surface changes demonstrated after excimer laser ablation may be indicative of temperature-induced transverse collagen fibril contraction and stress redistribution, or the ablation threshold of the stromal surface may be altered. This phenomenon may be of increased importance using lasers with increased thermal load.

Previous works showed a complex relationship between the temporal and spatial distribution of the laser spots [19]. The increase in the corneal surface temperature depends on the time sequences of the laser spots, the amount of correction, and the type of correction; i.e., myopic, hyperopic, or phototherapeutic keratectomy. The temporal and spatial positioning affects the temperature increase strongly. Scan sequences that allow a higher degree of temporal and spatial overlapping will lead to higher temperatures than spot sequences that avoid or minimize such overlapping. A thermal modeling of the temperatures at high repetition-rate heating was presented by Brygo et al. [20] In that study, laser beam absorption in

corneal tissue resulted in the matter heating and degradation at a sufficiently high temperature. The model developed by Brygo et al. [20] is considered to be purely thermal and linear. It is based on the 1-dimensional heat equation with constant coefficients. The general solution of the heat equation can be obtained in terms of the Green functions. The temperature for high-repetition-rate heating can be obtained using the linearity of the heat equation with constant coefficients. The heating and cooling at a high-repetition-rate are described by the sum of temperatures from positive intensities during the pulse and negative intensities between two pulses. During heating with  $n$  pulses, a temperature increase must be considered and a cooling effect between two pulses. Previous works demonstrate the complexity and dependence of the surface temperature on the temporal and spatial spot distribution on the cornea [19]. Increasing the amount of the refractive correction, the repetition rate of the laser system, or an increase of the radiant exposure will lead to an increase in the ocular surface temperature. A larger optical zone and smaller laser spots will decrease the ocular surface temperature.

As for the dependence with dioptric corrections; as Figures 8 and 9 show, there is a positive correlation of roughness with ablation depth. Higher dioptric powers (or wider optical zones) lead to deeper ablations (removing also a higher amount of volume), thus likely are associated to higher induction of roughness.

These researches substantiate the need for achieving a smoother surface in laser ablation for vision correction, for achieving higher fidelity in the post-operative outcomes. Smoothing agents and optimized energy distribution patterns have been explored to achieve smoother surfaces after laser ablation. Arba-Mosquera et al. [21] presented the dual fluence concept for the sequencing of laser shots in corneal ablation, for achieving higher fidelity and avoiding vacancies and roughness of the cornea. Lombardo et al. [22] examined the impact of smoothing agent (0.25% sodium hyaluronate) on postoperative roughness in porcine corneas subjected to Excimer laser photorefractive keratectomy, by means of atomic force microscopy. Images of the ablated stromal surface showed undulations and granule-like features on the ablated surface of the specimens. The specimens on which the smoothing procedure was performed (root-mean-square [RMS] rough:  $0.152 \pm 0.014 \mu\text{m}$ ) were more regular ( $p < 0.001$ ) than those on which PRK alone was performed (RMS rough:  $0.229 \pm 0.018 \mu\text{m}$ ).

Modelling approaches have been proposed in the past to study the ablation profiles and outcomes of the refractive surgery excimer lasers [23]. The predicted post-operative

corneal ablation shape, ablated volume, asphericity and spherical aberration varies across commercial laser platforms, as well as the relative contribution of ablation pattern designs and efficiency losses to the increased asphericity [24]. We tested the laser beam characteristics to define a set of parameters characterizing the laser beam profile that can optimize the roughness in ablation. The assessment of quality of vision is now an essential aspect of postoperative assessments following refractive procedures. Quality of vision is a subjective entity and the perception of quality of vision consists of various factors.

Plastic models have been used in refractive surgery research and calibration for a long time, especially for the assessment of roughness and calibration of pulse energy (radiant exposure or fluence) [1, 2, 5, 25, 26]. However, it has not been until recently that plastic models have been used to study in detail the changes in the shape of the flat or spherical surfaces, after refractive surgery [27, 28]. Ablating plastic model corneas not affected by biomechanical or other biological effects with clinical lasers, allows to directly measure the actual ablation pattern provided by the laser, avoiding the approximations and assumptions used in theoretical models. However, plastic models are not intended to mimic the response of the cornea but rather used to characterize the laser systems. The differences in ablation process between collagen and PMMA is well documented in the literature [11, 12, 29]. The cornea-to-PMMA ablation efficiency rate depends on the applied radiant exposure and the super-Gaussian order of the beam profile. As the radiant exposure increases, the cornea-to-PMMA ratio decreases. As the radiant exposure decreases approaching the ablation threshold for PMMA, the cornea-to-PMMA ratio increases. Below the ablation threshold for PMMA, the cornea-to-PMMA ablation efficiency rate cannot be calculated. As the super-Gaussian order increases, the cornea-to-PMMA ratio decreases. Maintaining the pulse energy constant, as the super-Gaussian order increases, the cornea-to-PMMA ratio may increase or decrease depending on the level of the total energy per pulse. As the ablation efficiency decreases towards periphery, the cornea-to-PMMA ablation ratio increases. From the ablation deviations observed in PMMA, the impact in deviations in corneal ablation can be estimated. The deviations in corneal ablation depend on the ablation deviations observed in PMMA, the nominally applied radiant exposure and the super-Gaussian order of the beam profile. For a given ablation deviation observed in PMMA, as the nominal radiant exposure increases, the relative corneal deviation increases. As the super-Gaussian order increases, the relative corneal deviation gains linearity, becoming linear for a flat-top energy profile. Additionally,

similar to other groups we found more roughness for deeper ablations in plastic models.

Several factors are associated with the epithelial response in refractive surgery [30–34]. An important aspect for consideration in postoperative refractive outcomes is the epithelial masking that will finish the smoothing process after the corneal ablation [35, 36]. An optimum topography of the stroma facilitates reepithelialization [37, 38]. Additionally, it is known that stromal topography affects overlying epithelial function including the differential expression of both cellular and extracellular substances [39]. Attempts have been made in the past to develop mathematical models used as the basis to design ablation patterns that compensate in advance for the expected corneal surface smoothing response [40–42].

In this work we performed eight PMMA tests (each with 12 ablations from  $-12D$  to  $+6D$ , accounting for a total of 96 ablations on PMMA) in a nonsequential settings procedure to avoid/reduce model bias; time drifts, hysteresis effects. To increase robustness not only  $8 \times 8$  analyses, but four vs. four cumulative analyses, as well as pairwise analyses have been included.

The effect of dithering was the largest, followed by truncation, and jitter had the lowest impact on results. So that: dithering approaches help to further minimize residual roughness after ablation; minimum (or no) truncation of the beam is essential to minimize residual roughness after ablation; and jitter shall be avoided to minimize residual roughness after ablation.

Interestingly the different test conditions not only affected roughness, but performance as well. The absence of pinhole; the use of ordered dithering; and the absence of jitter all enhanced performance. This can be explained by the fact that the best fit of a rougher shape runs somewhere between the peaks and the valleys of the rough surface. For smoother surfaces the difference from peak to valley reduces, so that the best fit line runs closer to the maximum envelop (peaks).

We found one “anomaly” in our results: The best condition derived from Figures 7 and 8 (and Table 2) should have been test setting 5 (without pinhole, with dithering, without jitter), but the actual empirical best condition (Figure 6) was test setting 4 (with pinhole, with dithering, and without jitter). There was no statistically significant difference in roughness between test settings 4 and 5 (empirical best vs. predicted best) (difference in roughness 0.1%;  $p = 0.5$ ).

Of the best 4 conditions (Table 2): three are without pinhole, three are with dithering, and three are without jitter. Pairwise comparisons confirm: the presence of pinholes is systematically worse than no truncation, dithering is systematically better than without dithering, and jitter is

systematically worse than without jitter. Once again confirming the robustness of the findings.

Based on the presented empirical results on PMMA, it can be foreseen that smoother surfaces would be achieved immediately after the ablation, using the proposed laser beam characteristics. This means at least two related potential advantages: (1) Short term outcomes may be better in the time period where the epithelium remodeling/smoothing/masking takes place, (2) Time for surface recovery may be shorter; since the surface is smoother to start with, epithelium may need less remodeling, which means less time for remodeling. Some other advantages of this model can be speculated or at least subjected to clinical assessment, namely, improving the smoothness seems a no risk condition, improvement in short term outcomes (without compromising long term ones), shorter recovery time to reach final visual acuity goal, higher levels of final visual acuity, shorter reepithelization time, reduced levels of induced higher order aberrations, and less haze response.

Regarding reepithelialization, these implications may be more relevant for PRK (surface procedure) than for subsurface procedures such as LASIK and small-lenticule extraction surgery (for which the epithelium remains largely intact during the treatment) [43]. Likely, ablation-surface roughness may play a larger role on epithelial remodeling after PRK versus LASIK and SMILE. Although postoperative epithelial remodeling has been reported after LASIK and SMILE procedures, as well [44].

The surface roughness is influenced by the formation of random or almost periodic holes with a depth of several  $\mu\text{m}$ . For high quality surface ablation, the formation of periodic structures and random holes should be avoided. This can be achieved by orienting the scan direction perpendicular to the polarization [45]. In order to minimize the surface roughness, Neuenschwander et al. [46] suggested that the optimum ratio between pulse distance and spot radius should be  $>1.0$ , and the ratio between the line distance and spot radius should be  $\approx 0.5$ . Domke et al. [44] explored the optimal combination of pulse-to-pulse distance and fluence in order to minimize the surface roughness for the ablation of silicon, irradiated using an ultrafast femtosecond laser. They concluded that the maximum specific ablation rate was achieved at fluence of about  $2 \text{ J/cm}^2$ . At a fluence of  $2.8 \text{ J/cm}^2$ , the global minimum of the surface roughness was determined to be about 220 nm at pulse distance =  $0.67 \times$  spot radius. The influence of the furrows on the surface roughness seemed to be negligible at this fluence. Their results suggest that the optimal pulse distance increases with fluence. The local ablation frequency and spot overlap has also shown to affect the surface roughness in PMMA [47, 48]. Bende et al. [49] used

a 1.0 mm Gaussian beam flying spot excimer laser to study the impact of spot overlap and ablation frequency on surface roughness in PMMA flat ablations (like PTK). They found that the surface roughness varies as a function of ablation depth, where the surface roughness for a PTK ablation in PMMA plates varied between 0.26 and 0.49  $\mu\text{m}$  for a 50  $\mu\text{m}$  deep ablation and 0.65–1.12  $\mu\text{m}$  for a 250  $\mu\text{m}$  deep ablation. In PMMA the minimal surface roughness was found for an overlap of 72.5%.

There is a delicate balance between the spot energy and spot diameter in terms of the roughness in ablation. Correcting the higher-order aberrations of the eye requires lasers with smaller spots and finer resolution [50]. It has been shown that a top-hat laser beam of 1.0 mm (Gaussian with full-width half maximum of 0.76 mm) is small enough to produce custom ablation for typical human eyes [51].

**Table 5:** Dual test settings: the values of various input parameters used in the ablation methodology. These values were retained in all the tests unless stated otherwise.

Parameter	Common parameters	
Repetition rate (Hz)	1050	
Full width half maximum (mm)	0.54	
Super Gaussian order (N)	1.27	
$R_0$ , beam size when the radiant exposure falls to $1/e^2$ its peak value (mm)	0.41	
Threshold ablation fluence ( $\text{mJ}/\text{cm}^2$ ) for human cornea	42	
Absorption coefficient for human cornea ( $\mu\text{m}^{-1}$ )	3.21	
Threshold ablation fluence ( $\text{mJ}/\text{cm}^2$ ) for PMMA	67	
Absorption coefficient for PMMA ( $\mu\text{m}^{-1}$ )	5.2	
Parameter	Default value	Test value
Truncation diameter (mm)/foot print (mm)	0.7	None
Spot energy (mJ)	0.75	0.9
Pinhole energy transmission (%)	76%	100%
Cut-off beam intensity at truncation (%)	27%	0%
Laser power (mW)	788	945
Peak radiant exposure ( $\text{mJ}/\text{cm}^2$ )	329	317
Corneal spot depth ( $\mu\text{m}$ )	0.64	0.63
Corneal spot size (mm)	0.7	0.82
Corneal spot volume (pl)	174	188
PMMA spot depth ( $\mu\text{m}$ )	0.31	0.30
PMMA spot size (mm)	0.7	0.74
PMMA spot volume (pl)	74	72
Dithering	None (heuristic reticular search)	Ordered (ordered dithering search)
Jitter ( $\mu\text{m}$ )	0	20

Several units for measuring the roughness in ablation have been proposed [5]. In our analysis, we used the RMS as unit to define roughness in ablation.

There are few limitations associated with our methods. Only one AMARIS was involved in the test, the truncation (pinhole) was tested for a single value (700  $\mu\text{m}$ ), only ordered predithering was tested, and jitter was tested for a single value (20  $\mu\text{m}$  in X/Y). Further to that no true Gaussian beam was tested, but a close-to-Gaussian beam profile was used for the various test settings. Similarly, PMMA performance was assessed, and not directly the corneal roughness. Finally, we applied predithering (anticipating errors), but also postdithering approaches (error diffusion) may be pursued.

The results show that the laser characteristics used in a corneal laser procedure have a major impact on the surface quality. The presence of pinholes truncating the beam induced extra roughness, the use of ordered dithering reduces residual roughness, and the presence of jitter induces extra roughness. From the results, a proper optimum configuration for minimizing the roughness in ablation for defined input parameters (Table 5) have been found specifically, no spot truncation (no pinhole); and using dithering strategies without jitter.

**Acknowledgements:** The authors acknowledge the support of Mr. Amin Seraji (employee at SCHWIND eye-tech-solutions, Kleinostheim, Germany) as a member of the team executing the tests.

**Author contributions:** Shwetabh Verma and Samuel Arba Mosquera are employees at SCHWIND eye-tech-solutions, Kleinostheim, Germany.

**Research funding:** None declared.

**Conflict of interest statement:** No other conflicts of interest.

## References

- [1] C. Argento, G. Valenzuela, H. Huck, G. Cremona, M. J. Cosentino, and M. F. Gale, "Smoothness of ablation on acrylic by four different excimer lasers," *J. Refract. Surg.*, vol. 17, no. 1, pp. 43–45, 2001.
- [2] A. V. Doga, A. A. Shpak, and V. A. Sugrobov, "Smoothness of ablation on polymethylmethacrylate plates with four scanning excimer lasers," *J. Refract. Surg.*, vol. 20, no. 5, pp. S730–S733, 2004.
- [3] M. Mrochen, U. Schelling, C. Wuellner, and C. Donitzky, "Influence of spatial and temporal spot distribution on the ocular surface quality and maximum ablation depth after photoablation with a 1050 Hz excimer laser system," *J. Cataract Refract. Surg.*, vol. 35, no. 2, pp. 363–373, 2009.

- [4] J. W. Thomas, S. Mitra, A. Z. Chuang, and R. W. Yee, "Electron microscopy of surface smoothness of porcine corneas and acrylic plates with four brands of excimer laser," *J. Refract. Surg.*, vol. 19, no. 6, pp. 623–628, 2003.
- [5] C. B. O'Donnell, J. Kemner, and F. E. O'Donnell, Jr., "Surface roughness in PMMA is linearly related to the amount of excimer laser ablation," *J. Refract. Surg.*, vol. 12, no. 1, pp. 171–174, 1996.
- [6] S. Arba-Mosquera and S. Verma, "Analytical optimization of the ablation efficiency at normal and non-normal incidence for generic super Gaussian beam profiles," *Biomed. Opt. Express*, vol. 4, no. 8, pp. 1422–1433, 2013.
- [7] S. Verma, J. Hesser, and S. Arba-Mosquera, "Optimum laser beam characteristics for achieving smoother ablations in laser vision correction," *Invest. Ophthalmol. Vis. Sci.*, vol. 58, no. 4, pp. 2021–2037, 2017.
- [8] C. W. Tyler, H. Chan, L. Liu, B. McBride, and L. L. Kontsevich, "Bit stealing: how to get 1786 or more gray levels from an 8-bit color monitor," in *Proc. SPIE 1666, Human Vision, Visual Processing, and Digital Display III*, vol. 1666, International Society for Optics and Photonics, 1992.
- [9] B. Bayer, "An optimum method for two-level rendition of continuous-tone pictures," *IEEE Int. Conf. Commun.*, vol. 1, pp. 11–15.
- [10] Smollins M. Lynbrook eye doctor recalls conducting first laser surgery (Posted April 5, 2018). Available at: <http://liherald.com/stories/30-years-later-lynbrook-eye-doctor-recalls-first-laser-surgery,101790>.
- [11] S. Arba-Mosquera and T. Klinner, "Improving the ablation efficiency of excimer laser systems with higher repetition rates through enhanced debris removal and optimized spot pattern," *J. Cataract Refract. Surg.*, vol. 40, no. 3, pp. 477–484, 2014.
- [12] S. Arba-Mosquera and N. Triefenbach, "Method for setting calibration data to control unit of laser ablation device, involves deriving new calibration data, and automatically storing new calibration data for control unit in laser ablation device," U.S. Patent DE 102 009 016 008 (B4), Nov. 28, 2013.
- [13] P. Pérez-Merino, M. C. Martínez-García, S. Mar-Sardaña, A. Pérez-Escudero, T. Blanco-Mezquita, A. Mayo-Iscar, and J. Merayo-Llodes, "Corneal light transmission and roughness after refractive surgery," *Optom. Vis. Sci.*, vol. 87, no. 7, pp. E469–E474, 2010.
- [14] P. Perez-Merino, C. Martinez-Garcia, S. Mar-Sardaña, A. Perez-Escudero, J. Merayo-Llodes, T. Blanco-Mezquita, and E. Garrido-Calvo, "Relationship between the roughness of corneal epithelium and the transmission of light," *Investig. Ophthalmol. Vis. Sci.*, vol. 49, p. 3910, 2008.
- [15] B. Bhushan, *Surface Roughness Analysis and Measurement Techniques*, Columbus, The Ohio State University.
- [16] F. E. Fantes and G. O. Waring, 3rd, "Effect of excimer laser radiant exposure on uniformity of ablated corneal surface," *Laser Surg. Med.*, vol. 9, no. 6, pp. 533–542, 1989.
- [17] S. A. Naroo and W. N. Charman, "Surface roughness after excimer laser ablation using a PMMA model: profilometry and effects on vision," *J. Refract. Surg.*, vol. 21, no. 3, pp. 260–268, 2005.
- [18] S. J. McCafferty, J. T. Schwiegerling, and E. T. Enikov, "Corneal surface asphericity, roughness, and transverse contraction after uniform scanning excimer laser ablation," *Invest. Ophthalmol. Vis. Sci.*, vol. 53, no. 3, pp. 1296–1305, 2012.
- [19] M. Mrochen, U. Schelling, C. Wuellner, and C. Donitzky, "Effect of time sequences in scanning algorithms on the surface temperature during corneal laser surgery with high-repetition-rate excimer laser," *J. Cataract Refract. Surg.*, vol. 35, pp. 738–746, 2009.
- [20] F. Brygo, A. Semerok, R. Oltra, J.-M. Weulersse, and S. Fomichev, "Laser heating and ablation at high-repetition-rate in thermal confinement regime," *Appl. Surf. Sci.*, vol. 252, pp. 8314–8318, 2006.
- [21] S. Arba-Mosquera and T. Hollerbach, "Ablation Resolution in Laser Corneal Refractive Surgery: The Dual Fluence Concept of the AMARIS Platform," *Advances in Optical Technologies*, vol. 2010, p. 13, 2010, Art no. 538541.
- [22] M. Lombardo, P. Maria, D. Santo, G. Lombardo, R. Barberi, and S. Serrao, "Roughness of excimer laser ablated corneas with and without smoothing measured with atomic force microscopy," *J. Refract. Surg.*, vol. 21, pp. 469–475, 2005.
- [23] K. Young, M. Choi, and S. Bott, "Impact of ablation efficiency reduction on post-surgery corneal asphericity: simulation of the laser refractive surgery with a flying spot laser beam," *Opt. Express*, vol. 16, no. 16, pp. 11808–11821, 2008.
- [24] C. Dorronsoro, L. Remon, J. Merayo-Llodes, and S. Marcos, "Experimental evaluation of optimized ablation patterns for laser refractive surgery," *Opt. Express*, vol. 17, no. 17, pp. 15292–15307, 2009.
- [25] J. D. Gottsch, E. V. Rencs, J. L. Cambier, D. Hall, D. T. Azar, and W. J. Stark, "Excimer laser calibration System," *J. Refract. Surg.*, vol. 12, no. 3, pp. 401–411, 1996.
- [26] A. M. Roszkowska, G. Korn, M. Lenzner, M. Kirsch, O. Kittelmann, R. Zatonski, P. Ferreri, and G. Ferreri, "Experimental and clinical investigation of efficiency and ablation profiles of new solid-state deepultraviolet laser for vision correction," *J. Cataract Refract. Surg.*, vol. 30, no. 12, pp. 2536–2542, 2004.
- [27] S. Marcos, C. Dorronsoro, and D. Cano, "Spherical aberration prevention method in e.g. laser refractivesurgery system," US Patent WO 2005/122873 A1, 2005.
- [28] C. Dorronsoro, D. Cano, J. Merayo-Llodes, and S. Marcos, "Experiments on PMMA models to predict the impact of corneal refractive surgery on corneal shape," *Opt. Express*, vol. 15, no. 12, pp. 7243–7244, 2007.
- [29] S. Arba-Mosquera and N. Triefenbach, "Analysis of the cornea-to-PMMA ablation efficiency rate," *J. Mod. Opt.*, vol. 59, no. 10, pp. 930–941, 2012.
- [30] C. A. Gauthier, B. A. Holden, D. Epstein, B. Tengroth, P. Fagerholm, and H. Hamberg-Nyström, "Factors affecting epithelial hyperplasia after photorefractive keratectomy," *J. Cataract Refract. Surg.*, vol. 23, no. 7, pp. 1042–1050, 1997.
- [31] C. P. Lohmann and J. L. Güell, "Regression after LASIK for the treatment of myopia: the role of the corneal epithelium," *Semin. Ophthalmol.*, vol. 13, no. 2, pp. 79–82, 1998.
- [32] S. E. Wilson, R. R. Mohan, J. W. Hong, J. S. Lee, R. Choi, and R. R. Mohan, "The wound healing response after laser in situ keratomileusis and photorefractive keratectomy: elusive control of biological variability and effect on custom laser vision correction," *Arch. Ophthalmol.*, vol. 119, no. 6, pp. 889–896, 2001.
- [33] M. A. Qazi, C. J. Roberts, A. M. Mahmoud, and J. S. Pepose, "Topographic and biomechanical differences between hyperopic and myopic laser in situ keratomileusis," *J. Cataract Refract. Surg.*, vol. 31, no. 1, pp. 48–60, 2005.

- [34] H. M. Woo, M. S. Kim, O. K. Kweon, D. Y. Kim, T. C. Nam, and J. H. Kim, "Effects of amniotic membrane on epithelial wound healing and stromal remodelling after excimer laser keratectomy in rabbit cornea," *Br. J. Ophthalmol.*, vol. 85, no. 3, pp. 345–349, 2001.
- [35] J. A. Moilanen, J. M. Holopainen, M. H. Vesaluoma, and T. M. Tervo, "Corneal recovery after lasik for high myopia: a 2-year prospective confocal microscopic study," *Br. J. Ophthalmol.*, vol. 92, no. 10, pp. 1397–1402, 2008.
- [36] B. Mulholland, S. J. Tuft, and P. T. Khaw, "Matrix metalloproteinase distribution during early corneal wound healing," *Eye*, vol. 19, no. 5, pp. 584–588, 2005.
- [37] P. Vinciguerra, C. Azzolini, and R. Vinciguerra, "Corneal curvature gradient determines corneal healing process and epithelial behavior," *J. Refract. Surg.*, vol. 31, no. 4, pp. 281–282, 2015.
- [38] P. Vinciguerra, C. J. Roberts, E. Albé, M. R. Romano, A. Mahmoud, S. Trazza, and R. Vinciguerra, "Corneal curvature gradient map: a new corneal topography map to predict the corneal healing process," *J. Refract. Surg.*, vol. 30, no. 3, pp. 202–207, 2014.
- [39] H. G. Dierick and L. Missotten, "Is the corneal contour influenced by a tension in the superficial epithelial cells? A new hypothesis," *Refract. Corneal Surg.*, vol. 8, no. 1, pp. 54–59, 1992.
- [40] M. Tang, "Corneal Mean Curvature Mapping: Applications in Laser Refractive Surgery, Columbus," The Ohio State University.
- [41] D. Huang, M. Tang, and R. Shekhar, "Mathematical model of corneal surface smoothing after laser refractive surgery," *Am. J. Ophthalmol.*, vol. 135, no. 3, pp. 267–278, 2003.
- [42] D. M. Lieberman and J. W. Grierson, "A mathematical model for laser in situ keratomileusis and photorefractive keratectomy," *J. Refract. Surg.*, vol. 16, no. 2, pp. 177–186, 2000.
- [43] P. Vinciguerra, M. Azzolini, P. Airaghi, P. Radice, and V. De Molfetta, "Effect of decreasing surface and interface irregularities after photorefractive keratectomy and laser in situ keratomileusis on optical and functional outcomes," *J. Refract. Surg.*, vol. 14, no. 2, pp. S199–S203, 1998.
- [44] P. Khamar, R. Chandapura, R. Shetty, Z. Dadachanji, G. Kundu, Y. Patel, R. M. M. A. Nuijts, and A. Sinha Roy, "Epithelium Zernike indices and artificial intelligence can differentiate epithelial remodeling between flap and flapless refractive procedures," *J. Refract. Surg.*, vol. 36, no. 2, pp. 97–10, 2020.
- [45] M. Domke, G. Piredda, J. Zehetner, and S. Stroj, "Minimizing the surface roughness for silicon ablation with ultrashort laser pulses," *J. Laser Micro/Nanoengineering*, vol. 11, no. 1, pp. 100–103, 2016.
- [46] B. Neuenschwander, G. F. Bucher, G. Hennig, C. Nussbaum, B. Joss, M. Mural, S. Zehnder, U. W. Hunziker, and P. Schütz, in *International Congress on Applications of Lasers & Electro Optics (ICALEO)*, 2010, p. 707.
- [47] A. M. Khalid Hafiza, E. V. Bordatchev, and R. O. Tutunea-Fatan, "Influence of overlap between the laser beam tracks on surface quality in laser polishing of AISI H13 tool steel," *J. Manuf. Process.*, vol. 14, no. 4, pp. 425–434, 2012.
- [48] A. K. Gardner, M. Staninec, and D. Fried, "The influence of surface roughness on the bond strength of composite to dental hard tissues after Er:YAG laser irradiation," *Laser Dent.*, vol. XI, p. 144, 2005.
- [49] T. Bende, S. Becker, T. Oltrup, R. Berret, and B. Jean, "Influence of the overlap of a 1.0 mm gaussian beam flying spot excimer laser on surface roughness," in *ARVO Annual Meeting Abstract*, 2003.
- [50] D. Huang and M. Arif, "Spot size and quality of scanning laser correction of higher order wavefront aberrations," *J. Refract. Surg.*, vol. 17, pp. S588–S591, 2001.
- [51] A. Guirao, D. R. Williams, and S. M. MacRae, "Effect of beam size on the expected benefit of customized laser refractive surgery," *J. Refract. Surg.*, vol. 19, pp. 15–23, 2003.